Effect of Si-doping on the structure and conductivity of (Sr/Ca)$_2$MnFeO$_{6-\delta}$ systems

Smith, Alaric; James, Matthew; Slater, Peter

Document Version
Peer reviewed version

Link to publication on Research at Birmingham portal

Effect of Si-doping on the Structure and Conductivity of $(Sr/Ca)_2MnFeO_{6-\delta}$ Systems

A.D. Smith[a], M. S. James,[a] P. R. Slater,[a]

[a.] School of Chemistry, University of Birmingham, Birmingham, United Kingdom, B15 2TT.

Following previous work on silicate doping of perovskite $(Sr/Ca)MnO_3$ and $(Sr/Ca)FeO_{3-\delta}$ materials for potential application as electrode materials for solid oxide fuel cells, here we report the successful incorporation of silicon into the mixed Mn/Fe systems, $(Sr/Ca)_2MnFeO_{6-\delta}$. The results show a higher level of Si doping to be possible for $Ca_2MnFe_{1-x}Si_xO_{6—\delta}$ ($0 \leq x \leq 0.4$) compared to $Sr_2MnFe_{1-x}Si_xO_{6—\delta}$ ($0 \leq x \leq 0.2$). In both cases, the conductivity is improved for low doping levels ($x \leq 0.1$), with a subsequent decrease for higher doping levels. Additional preliminary work has shown that phosphate can also be successfully incorporated into these perovskite systems. The work therefore further illustrates the potential of oxyanion doping in perovskite systems of interest for Fuel Cell applications.

Introduction

Research into solid oxide fuel cells and electrolysers (SOFC and SOE) has focused significantly on the development of perovskite systems (ABO_3) which have mixed ionic-electronic conduction for applications as electrode materials. Traditionally, the optimisation of the properties of these materials has focused on doping on the A- and/or B-cation site with ions of similar size, e.g. $La_{1-x}Sr_xMnO_{3-\delta}$, $La_{1-x}Sr_xCo_{1-y}Fe_yO_{3-\delta}$ and $Ba_{1-x}Sr_xCo_{1-y}Fe_yO_{3-\delta}$ (1-5). The perovskite structure is, however, far more flexible towards doping, and we have shown that oxyanions, such as phosphate, sulphate, silicate, borate, carbonate, can be incorporated into perovskite systems. In this doping strategy, the central "cation" (P, S, Si, B, C) occupies the B cation site, with the oxygens from the oxyanion group occupying either 3 (carbonate, borate) or 4 (phosphate, silicate, sulphate) of the 6 available oxygen positions around this site, with appropriate displacement to achieve the trigonal planar/tetrahedral coordination of the oxyanion (69). Silicon (as the silicate group) is an interesting example, since this has been previously considered a poison for SOFC's, especially with fluorite electrolyte materials (10-12). This can be correlated with the fact that the fluorite structure can accommodate very little silicon and so it will typically collect at grain boundaries, reducing the oxide ion conductivity. In contrast, perovskite materials can accommodate significant levels of Si, as illustrated by previous work on the incorporation of Si into $SrMnO_3$ and $CaMnO_3$ (up to 20% Si on the Mn site for $SrMnO_3$). In this prior work, it was shown that the Si doping improved the electronic conductivity both through electron doping (through the introduction of oxide ion vacancies, associated with the lower coordination number of Si (CN=4) versus Mn (CN=6)), and a stabilisation of the cubic perovskite structure for Si doped $SrMnO_3$ (13-15). Silicon has also incorporated

successfully into $SrFeO_{3-\delta}$ showing a change from a tetragonal to a cubic cell, along with good conductivity and stability (16-20).

In this paper we extend these silicon doping studies to examine the effect of Si incorporation into the mixed Mn/Fe system, $(Sr/Ca)_2MnFeO_{6-\delta}$, in order to investigate the effect on conductivity, for potential use as a low-cost SOFC cathode material. Previously, the structures and conductivities of undoped $(Sr/Ca)_2MnFeO_{6-\delta}$ have been investigated by a number of groups (21-25), but this is the first examination of the effect of Si doping. We show that Si can be successfully incorporated into these $(Sr/Ca)_2MnFeO_{6-\delta}$ systems, and report the conductivities of these doped phases. Preliminary results for phosphate doping in these systems are also reported.

Experimental

High purity $SrCO_3$, $CaCO_3$, MnO_2, Fe_2O_3 and SiO_2 were used to prepare, $Sr_{2-y}Ca_yMnFe_{1-x}Si_xO_{6-\delta}$ (y=0, 2) samples. Stoichiometric mixtures of the powders were intimately ground and initially heated to 1000 ºC (10 ºC / min) for 12 hours. Samples were then reground and heated to 1250 ºC (y=2), 1275 ºC (y=0) for 24 hours with an intermediate regrind. To ensure maximum oxygen content, the resulting samples were held at 350 ºC for 12 hours in air.

Powder X-ray diffraction data were collected in order to determine lattice parameters and phase purity of samples. Data were collected on Bruker D8 and D5005 diffractometers with Cu Kα radiation. The GSAS2 suite of programs was used to determine unit cell parameters (26).

Samples were also analysed using thermogravimetric analysis (Netzch STA 449 F2 Jupiter Thermal Analyser). Samples were heated to 1200 ºC (10 ºC / min) in N_2 and held at this temperature for 30 minutes to reduce the iron and manganese oxidation states to +3 and thus allow the oxygen content and average metal oxidation state to be determined.

Pellets for conductivity measurements were prepared by ball-milling (350 rpm for 30 minutes) before pressing samples into compacts and sintering at the synthesis temperature for 12 hours. Four Pt electrodes were attached with Pt paste and the samples heated to 950 ºC for 1 hours in air to ensure good contact. Samples were then cooled to 350 ºC and held at this temperature for 12 hours to ensure the maximum oxygen content. Conductivities were then measured in air with varying temperature using the four-probe dc method.

SEM images were collected on a Hitachi Tabletop Microscope TM4000Plus with EDS Oxford Instruments MICSF+ X-stream-2 attachment. The samples were analysed using energy-dispersive X-ray spectroscopy to determine the elemental distribution of the silicon across the sample

Results and Discussion

X-ray Diffraction Results

$Ca_2MnFe_{1-x}Si_xO_{6-\delta}$. The synthesis of silicon-doped $Ca_2MnFeO_{6-\delta}$ was examined, and single phase $Ca_2MnFe_{1-x}Si_xO_{6-\delta}$ samples were observed for $0 \leq x \leq 0.4$ (Figure 1), with higher levels of Si leading to impurity peaks, attributed to Ca_2SiO_4.
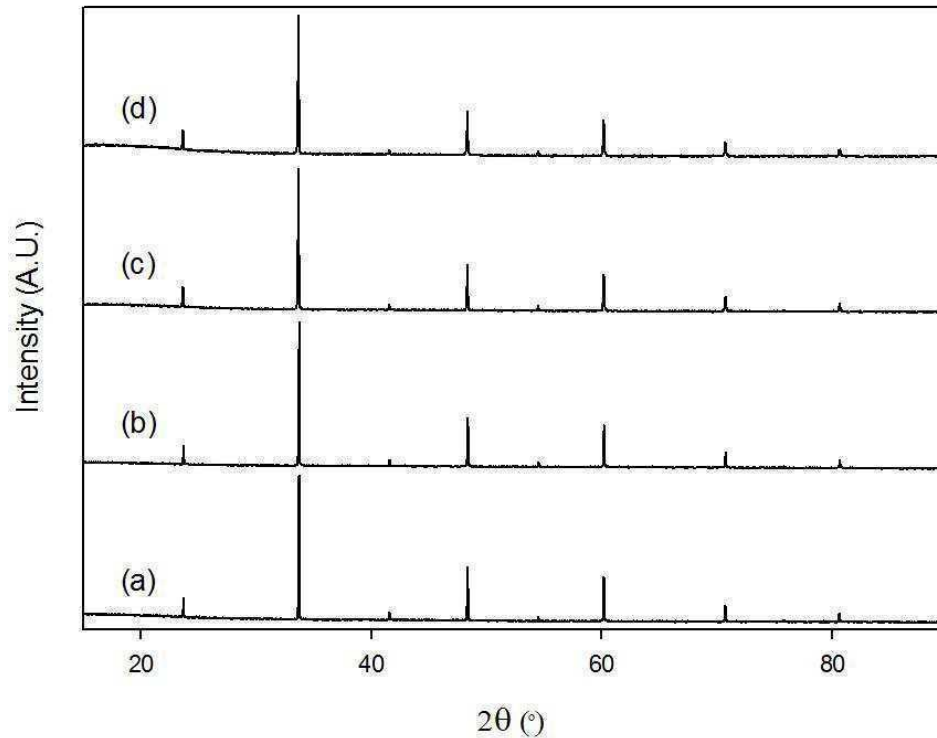

Figure 1. Powder X-ray diffraction patterns for (a) $Ca_2MnFe_{0.95}Si_{0.05}O_{6-\delta}$, (b) $Ca_2MnFe_{0.9}Si_{0.1}O_{6-\delta}$, (c) $Ca_2MnFe_{0.8}Si_{0.2}O_{6-\delta}$ and (d) $Ca_2MnFe_{0.6}Si_{0.4}O_{6-\delta}$ showing the formation of single phase perovskite samples.

In order to provide further confirmation of the successful incorporation of Si, an equivalent Fe deficient sample, $Ca_2MnFe_{0.8}O_{6-\delta}$ without SiO_2 addition, was prepared.

Unlike $Ca_2MnFe_{0.8}Si_{0.2}O_{6-\delta}$, the X-ray diffraction pattern for $Ca_2MnFe_{0.8}O_{6-\delta}$ indicated that the latter was not single phase (Figure 2), thus confirming the Si incorporation into the perovskite structure for $Ca_2MnFe_{0.8}Si_{0.2}O_{6-\delta}$.
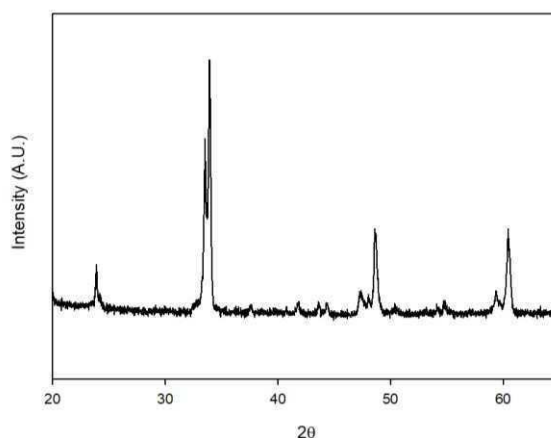
Figure 2. Powder X-ray diffraction data of $Ca_2MnFe_{0.8}O_{6-\delta}$ illustrating that without SiO_2 addition, a single phase cubic perovskite is not obtained.

Thermogravimetric analysis was used to determine the oxygen content and thus calculate the average oxidation state of the B-site metal cations. The results in Table 1 suggests a small increase in oxygen content on silicon doping.

TABLE I. Oxygen content and average B-site metal oxidation state for Ca2MnFe1-xSixO6-δ.

x	% Mass Loss	Oxygen Content	Average B-site Metal Oxidation State
0.05	1.86	5.34	3.33
0.1	1.92	5.38	3.35
0.2	1.71	5.39	3.32
0.4	1.57	5.46	3.33

Cell parameters for these samples were determined by Rietveld refinement (space group of *P m -3 m*). The manganese, iron and silicon were all placed on the B cation site in the expected stochiometric amounts. Cell parameters and goodness of fit values are presented in Table 2. An example fit showing observed, calculated and difference plots is presented in Figure 5.

TABLE II. Cell parameters and goodness of fit values for $Ca_2MnFe_{1-x}Si_xO_{6-\delta}$.

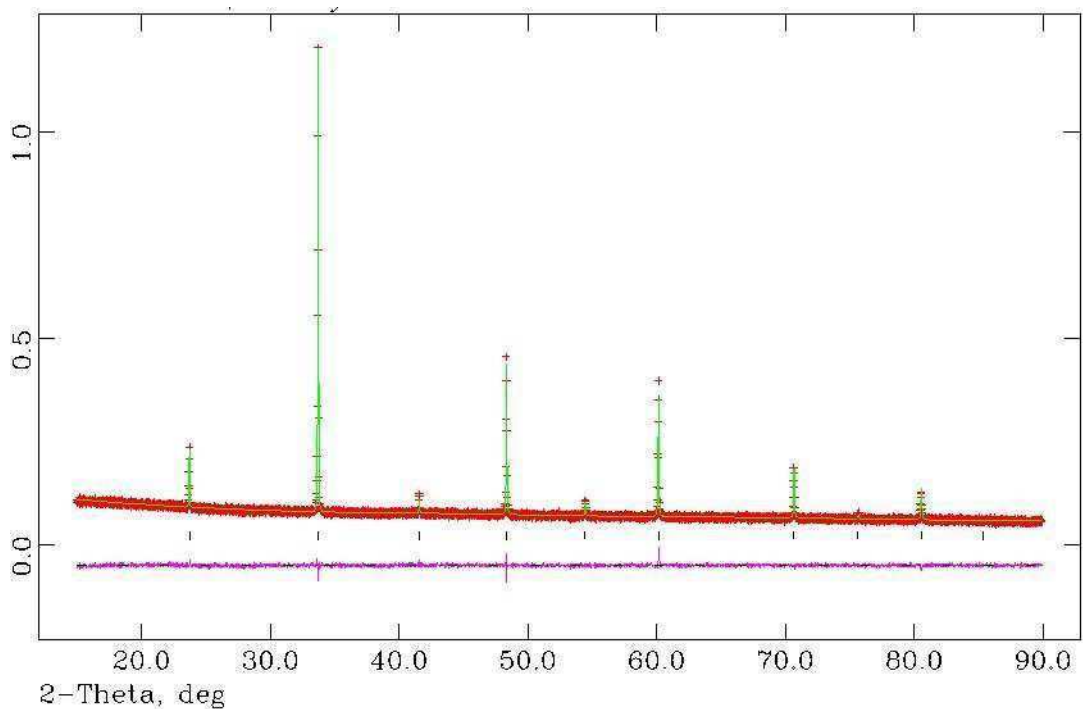| x	a (Å)	wRp	Rp	χ^2
0.05	3.77171(5)	3.05%	2.40%	1.063
0.1	3.77162(4)	3.04%	2.38%	1.200
0.2	3.77399(4)	3.87%	3.07%	1.144
0.4	3.77584(4)	4.21%	3.32%	1.099

Figure 3. Observed, calculated and difference plots for structural refinement of $Ca_2MnFe_{0.8}Si_{0.2}O_{5.39}$ using X-ray powder diffraction data.

The lattice parameters show a slight increase in cell volume with increasing Si content. As the TGA data suggest that the average transition metal oxidation state is approximately constant, this increase in volume may correlate with an increase in oxygen content on the introduction of Si^{4+} in place of Mn/Fe (average oxidation state ≈3.3+)

$\underline{Sr_2MnFe_{1-x}Si_xO_{6-\delta.}}$ Powder X-ray diffraction data (figure 4) confirmed that undoped $Sr_2MnFeO_{6-\delta}$ is a cubic perovskite in agreement with Nakahara et al.[21]
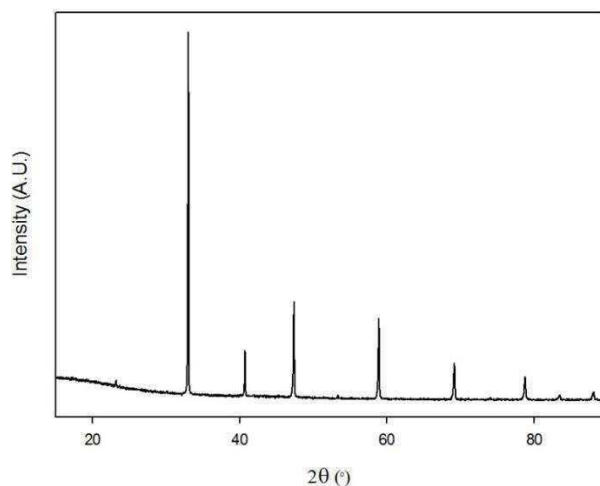

Figure 4. Powder X-ray diffraction data of $Sr_2MnFeO_{6-\delta}$ showing formation of a single phase cubic perovskite.

In this case the synthesis of silicon-doped $Sr_2MnFe_{1-x}Si_xO_{6-\delta}$ was successful for x≤0.2, with all samples in this range showing formation of a single-phase cubic perovskite (Figure 5).
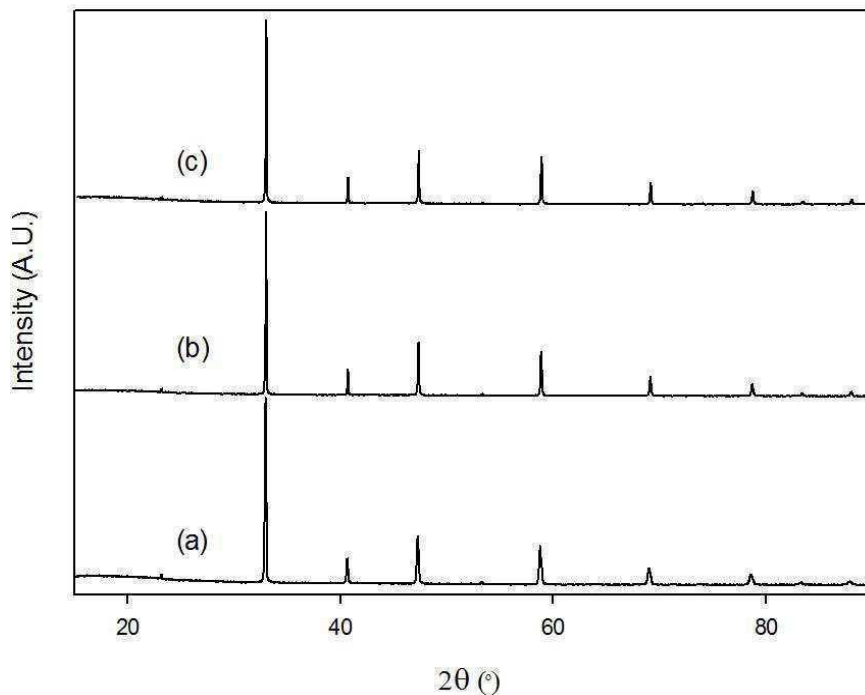
Figure 5. Powder X-ray diffraction data of (a) $Sr_2MnFe_{0.95}Si_{0.05}O_{6-\delta}$, (b) $Sr_2MnFe_{0.9}Si_{0.1}O_{6-\delta}$, (c) $Sr_2MnFe_{0.8}Si_{0.2}O_{6-\delta}$ showing formation of single phase cubic perovskites.

An equivalent Fe deficient sample, $Sr_2MnFe_{0.8}O_{6-\delta}$ without SiO_2 addition was prepared, in order to provide further confirmation of the successful incorporation of Si. As for the Ca series above, the X-ray diffraction pattern for $Sr_2MnFe_{0.8}O_{6-\delta}$ indicated that the sample was not single phase (Figure 6), thus confirming the Si incorporation into the perovskite structure for $Sr_2MnFe_{0.8}Si_{0.2}O_{6-\delta}$.

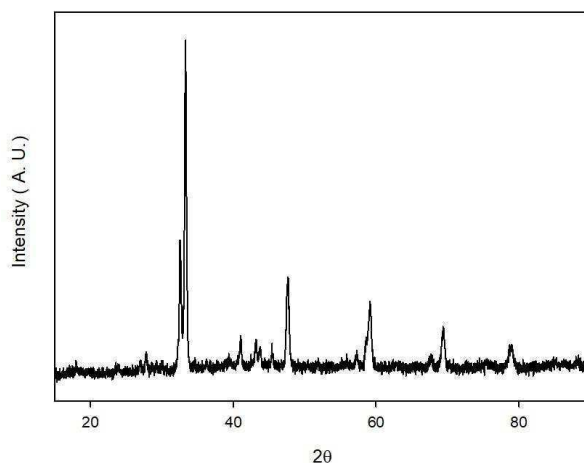Figure 6. Powder X-ray diffraction of $Sr_2MnFe_{0.8}O_{6-\delta}$ illustrating that without SiO_2 addition, a single phase cubic perovskite is not obtained.

Thermogravimetric analysis was used to determine the oxygen content and so calculate the average oxidation state of the B-site metal cations. Unlike the Ca series, the results (Table 3) suggest no systematic trend in oxygen content on silicon doping.

TABLE III. Oxygen content and B-site metal oxidation state for $Sr_2MnFe_{1-x}Si_xO_{6-\delta}$.

x	% Mass Loss	Oxygen Content	Average B-site Metal Oxidation State
0	2.22	5.52	3.52
0.05	1.91	5.47	3.46
0.1	2.10	5.54	3.51
0.2	1.41	5.42	3.36

Cell parameters for these samples were determined by Rietveld refinement (space group *P m -3 m*) similar to the Ca series. The final refined cell parameters and goodness of fit values are presented in Table 4. An example fit showing observed, calculated and difference plots is presented in Figure 7.

TABLE IV. Cell parameters and goodness of fit values for $Sr_2MnFe_{1-x}Si_xO_{6-\delta}$

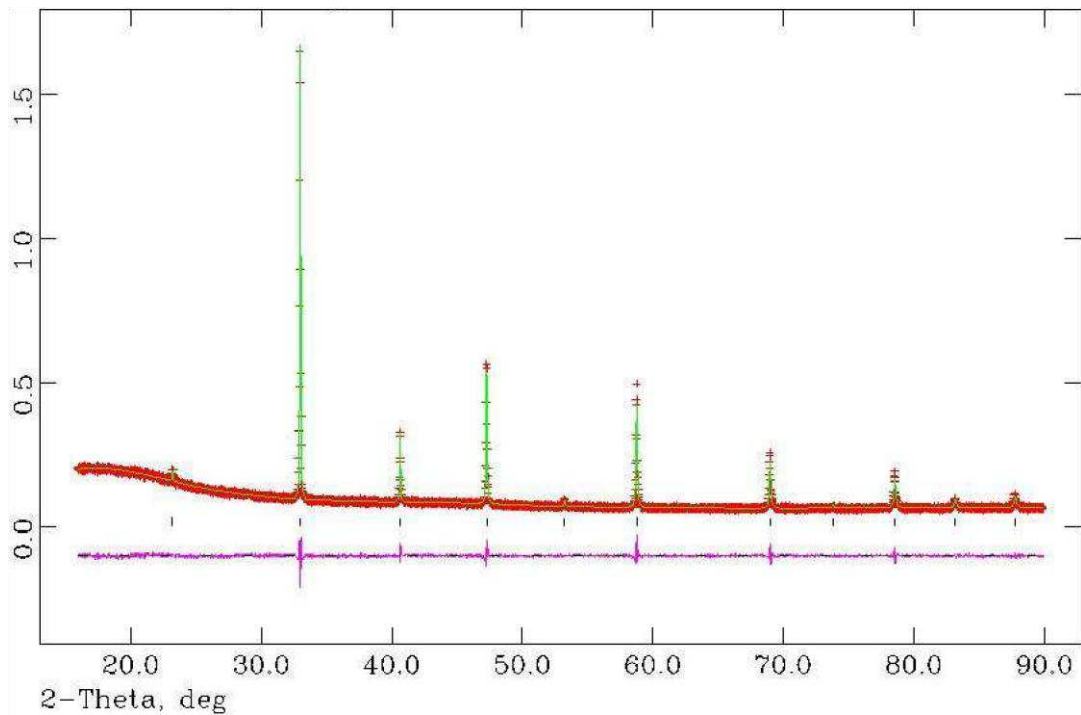| x	a(Å)	wRp	Rp	χ^2
0	3.84527(5)	3.44%	2.55%	2.125
0.05	3.84363(4)	3.66%	2.62%	1.836
0.1	3.85107(2)	3.40%	2.61%	1.345
0.2	3.85502(5)	4.26%	3.17%	1.762

Figure 7. Observed, calculated and difference plots for structural refinement of $Sr_2MnFe_{0.8}Si_{0.2}O_{5.43}$ using X-ray powder diffraction data.

The lattice parameters show a small increase for the higher Si contents, similar to the Ca series.

<u>Conductivity Measurements</u>

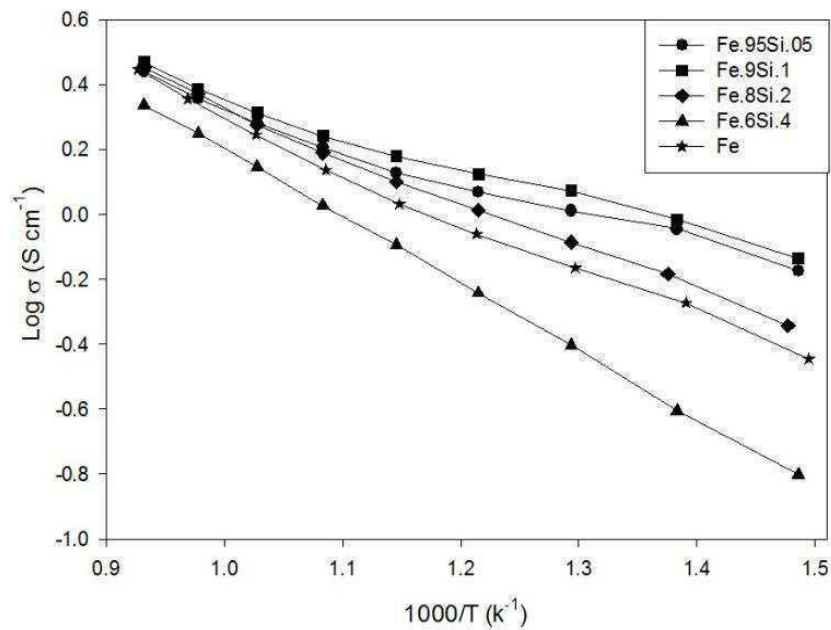$Ca_2MnFe_{1-x}Si_xO_{6-\delta}$ Conductivities in air for the $Ca_2MnFe_{1-x}Si_xO_{6-\delta}$ series are shown in figure 8.

Figure 8. Temperature dependence of the electronic conductivity for $Ca_2MnFe_{1-x}Si_xO_{6-\delta}$.

Similar to prior work on Si doping in $CaMnO_3$ [9], the data show an initial improvement in the conductivity with incorporation of silicon up to x = 0.1, compared to the undoped composition. However, the conductivity appears to decrease upon further Si incorporation, dropping beneath that of undoped $Ca_2MnFeO_{6-\delta}$ for the highest Si content sample, $Ca_2MnFe_{0.6}Si_{0.4}O_{6-\delta}$, which most likely relates to the high Si content beginning to disrupt the Mn/Fe-O network.

$\underline{Sr_2MnFe_{1-x}Si_xO_{6-\delta}.}$ Conductivities in air for the $Sr_2MnFe_{1-x}Si_xO_{6-\delta}$ series are shown in Figure 9.
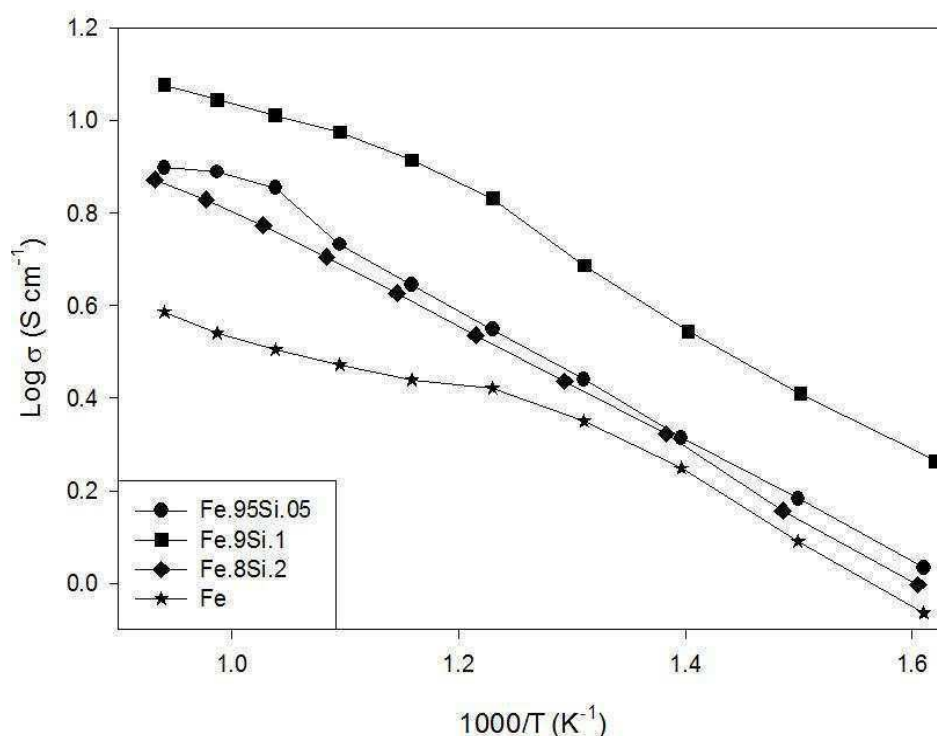

Figure 9. Temperature dependence of the electronic conductivity data for $Sr_2MnFe_{1-x}Si_xO_{6-\delta.}$

As for the Ca series and prior work on Si doping in $SrMnO_3$ [17], the data show an initial improvement in the conductivity on Si doping up to x = 0.1. However, the conductivity decreased upon further Si incorporation, albeit remaining still above that of undoped $Sr_2MnFeO_{6-\delta}$.

Stability in Low $p(O_2)$ Conditions

In order to evaluate, whether these materials might also be of interest as SOFC anode materials, preliminary studies on the stability of the samples in low $p(O_2)$ was performed. Samples were therefore heated under a 5%H_2 /95% N_2 atmosphere for 12 hours. All samples were shown to decompose after heating at 900 ºC, although they were shown to stable at lower temperatures (600 ºC). Further work in this area is in progress.

Scanning Electron Microscopy Analysis

Silicon doped $(Sr/Ca)_2MnFeO_{6-\delta}$ samples were compared using SEM with undoped, deficient $(Sr/Ca)_2MnFe_{1-x}O_{6-\delta}$ samples mixed with SiO_2 powder. The single phase Si doped samples $(Sr/Ca)_2MnFe_{1-x}Si_xO_{6-\delta}$ demonstrated a uniform distribution of silicon throughout the sample reinforcing that the silicon is fully incorporated within the perovskite structure. In comparison, the data for the mixture of Fe deficient $(Sr/Ca)_2MnFe_{1-x}O_{6-\delta}$ and SiO_2 powder show large clusters of SiO_2 are on the surface (Figure 10).
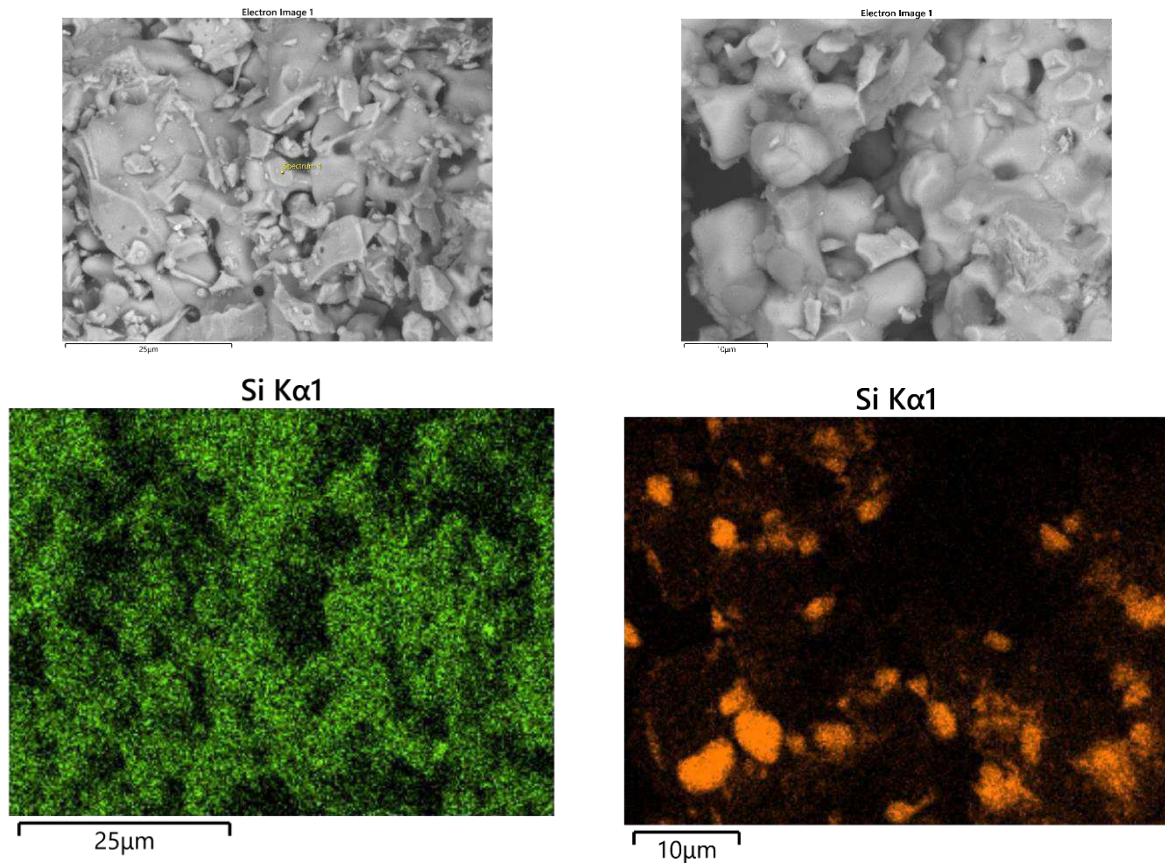
Figure 10. Top; Scanning electron microscope images of (left) $Ca_2MnFe_{0.8}Si_{0.2}O_{6-\delta}$ and (right) $Ca_2MnFe_{0.8}O_{6-\delta} + 0.2SiO_2$. Bottom; Energy-dispersive X-ray spectroscopy imaging of Si ($K\alpha1$) content (left) $Ca_2MnFe_{0.8}Si_{0.2}O_{6-\delta}$ and (right) $Ca_2MnFe_{0.8}O_{6-\delta} + 0.2SiO_2$.

Extension to Phosphate Doping

We have started to investigate doping these mixed Mn/Fe perovskite systems with other oxyanions in order to assess the effect on stability and conductivity. These preliminary studies indicate that phosphate can also be successfully incorporated into $Sr_{2x}Ca_xMnFeO_{6-\delta}$ giving single phase samples with a cubic perovskite cell, Figure 11. Cell parameters obtained from the Rietveld refinements are shown in Table 5. Further work is planned to determine the effect of this phosphate doping on the conductivity and stability.

TABLE V. Cell and goodness of fit parameters for $Sr_{2-x}Ca_xMnFe_{0.85}P_{0.15}O_{6-\delta}$.

x	a (Å)	Rwp	Rexp	χ^2
0	3.7755(9)	4.07%	2.68%	1.52
1	3.8161(4)	4.31%	2.64%	1.63
2	3.8510(7)	5.01%	2.74%	1.83
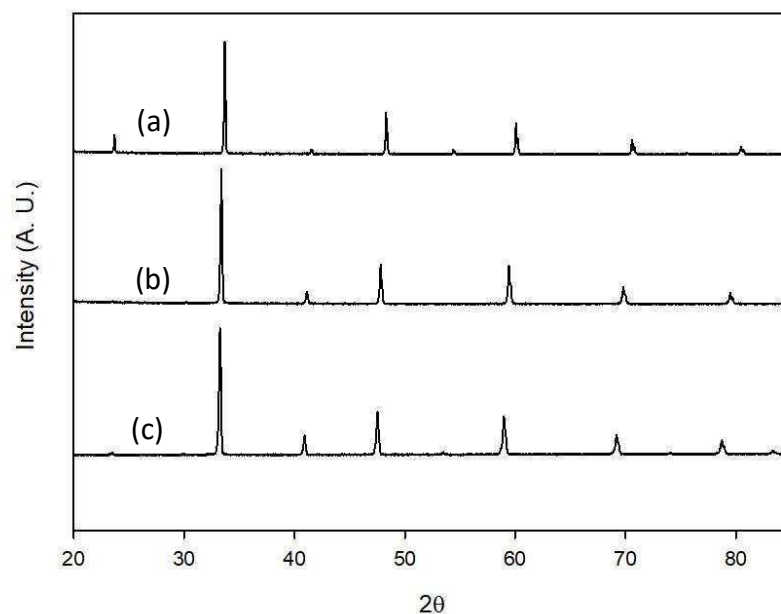
Figure 11. X-ray diffraction data for (a) $Ca_2MnFe_{0.85}P_{0.15}O_{6-\delta}$, (b) $SrCaMnFe_{0.85}P_{0.15}O_{6-\delta}$, (c) $Sr_2MnFe_{0.85}P_{0.15}O_{6-\delta.}$

Conclusions

Powder X-ray diffraction data have shown that silicon can be successfully doped into $Ca_2MnFe_{1-x}Si_xO_{6-\delta}$ ($0\leq x\leq0.4$) and $Sr_2MnFe_{1-x}Si_xO_{6-\delta}$ ($0\leq x\leq0.2$), resulting in the formation of a single phase cubic perovskites. For both systems, the conductivities are improved for low levels of Si doping ($x\leq0.1$), with a subsequent decrease at higher levels. Preliminary further work has shown that phosphate can also be incorporated into these systems. The work therefore shows that oxyanion doping represents another avenue for the modification of the structure and performance of perovskite systems. Furthermore, in addition to interest in the solid oxide fuel cell field, these systems are also attracting interest for use in alkaline fuel cells (27).

Acknowledgements

References

1. A. Orera and P. R. Slater, *Chem. Mat.*, **22**, 675-690. (2010)
2. A. J. Jacobson, *Chem. Mat.,* **22**, 660-674. (2010)
3. A. Lashtabeg and S. J. Skinner, *J. Mater. Chem.,* **16**, 3161-3170 (2006)
4. J. H. Kuo, H. U. Anderson and D. M. Spalin, *J. Solid State Chem.,* **87** 55-63. (1990)
5. H. Yokokaw, N. Sakai, T. Kawada and M. Dokiya, *Solid State Ion.,* **40-1,** 398401. (1990)

6. J. Deakin, I.Trussov, A. Gibbs, E. Kendrick and P. R. Slater, *Dalton Trans.,* **47,** 12901-12906 (2018)
7. A. Jarvis and P. R. Slater, *Crystals,* **7,** 169 (2017)
8. D. Perez-Coll, J. C. Perez-Flores, N. Nasani, P. R. Slater and D. P. Fagg, *J. Mater. Chem. A.* **4,** 11069-11076 (2016)
9. C. A. Hancock, J. M. Porras-Vazquez, P. J. Keenan and P. R. Slater., *Dalton Trans.,* **44,** 10559-10569 (2015)
10. D. Ivanova, E. Lima, A. Kovalevsky, F. M. L. Figueiredo, V. V. Kharton and F. M. B. Marques, *Ionics,* **14,** 349-356. (2008)
11. X. Guo and R. Waser, *Prog, Mater, Sci.,* 2006, **51,** 151-210
12. M. J. Verkerk, A. J. A. Winnubst and A. J. Burggraaf, *J. Mater Sci.,* **17,** 31133122 (1982)
13. S. P. S. Bedwal and J. Drennan, *J. Mater. Sci.,* **22,** 3231-3239. (1987)
14. M. L. Mecartney, *J. Am. Ceram. Soc.,* **70,** 54-58 (1987)
15. S. P. S. Bedwal and J. Drennan, *J. Mater. Sci.*, **24,** 88-96 (1989)
16. D. Ivanova, A. Kovalevsky, V. V. Kharton and F. M. B. Marques, *Boletin De La Sociedand Espanola De Ceramica Y Vidrio,* **47,** 201-206 (2008)
17. C. A. Hancock and P.R. Slater, Dalton Transactions, **40,** 5599-5603. (2011) 18. J. M Porras-Vazquez, E. R. Losilla, P. J. Keenn, C. A. Hancock, T.F Kemp, J. V. Hanna and P. R. Slater, *Dalton Transactions,* **42,** 5421-5429 (2013) 19. J. M. Porras-Vazquez, T. F. Kemp, J. V. Hanna and P. R. Slater, *J. Mater. Chem.,* **22,** 8287-8293 (2012)
20. J. M. Porras-Vazquez, T, Pike, C. A. Hancock, J. F. Marco, F. J. Berry and P. R. Slater, *Journal of Materials Chemistry A,* **1,** 11834-11841. (2013)
21. Y. Nakahara, S. Kato, M. Sugai, Y. Ohshima and K. Makino, *Mater. Lett.,* **30,** 163-167. (1997)
22. F. Ramezanipour, B. Cowie, S. Derakhsan, J. E. Greedan and L. M. D. Cranswick, *J. Solid State Chem.,***182,** 153-159 (2009)
23. F. Ramezanipour, J.E Greedan, L. M. D. Cranswick, V. O. Garlea, R. L. Donaberger and J. Siewenie, *J. Am. Chem. Soc.,* **134,** 3215-3227 (2012
24. S. Mulmi, R Hona, J Jasinski, F Ramezanipour, *J. Solid. State. Electrochem.,* **22,** 2329-2338 (2018)
25. R. V. Coates and J. W. McMillan, *Journal of Applied Chemistry,* **14,** 346, (1964)
26. B. H. Toby and R. B. Von Dreee, *J. Appl. Crystallogr.* **46,** 544-549 (2013)
27. Y.L. Zhu, W. Zhou, J. Sunarso, Y.J. Zhong, Z.P. Shao, *Adv Funct. Mater* **26**, 5862-5872 (2016).